Research article

Journal of RAMAN SPECTROSCOPY

Received: 30 May 2016 Revised: 20 October 2016 Accepted: 21 October 2016 Published online in Wiley Online Library: 21 November 2016

(wileyonlinelibrary.com) DOI 10.1002/jrs.5064

Raman spectroscopy of layered lead tin disulfide ($PbSnS_2$) thin films

Anna Łapińska,[a†] Andrzej Taube,[a,c†] Michał Wąsik,[a] Grażyna Zofia Żukowska,[b] Anna Duzynska,[a] Jarosław Judek[a] and Mariusz Zdrojek[a]*

Nowadays, the attention of researchers is focused on the large family of chalcogenides that poses very unique and interesting properties. One of them is the teallite – $PbSnS_2$, almost unrevealed ternary compound, promising thermoelectric material. In this work, we present first detailed Raman studies of $PbSnS_2$, including the polarization-dependent and temperature-dependent measurements (80–400 K range). The strong effect of polarization angle and temperature on the Raman spectra was observed. The polarization studies allowed to assign symmetry of observed modes. The temperature evolutions of the Raman spectra were explained by optical phonon decay into two or three acoustic phonons with equal energies. The extracted first-order temperature coefficients are among the largest reported so far for layered materials. Our results might be helpful in understanding the anisotropic optical, thermal and electrical properties of $PbSnS_2$. **Copyright © 2016 John Wiley & Sons, Ltd.**

Additional supporting information may be found in the online version of this article at the publisher's web site.

Keywords: lead tin disulfide; $PbSnS_2$; layered materials; anisotropy; thermal properties

Introduction

With the discovery of graphene and examination of its fundamental properties,[1,2] a renaissance of interest in layered materials has been started, including transition metal chalcogenides[3–6] and recently black phosphorus.[7] Moreover, regularly, new members of this compound family are reported or rediscovered.[8,9] The lead tin sulfide – $PbSnS_2$, a IV–VI-layered ternary semiconductor – is an example of not fully explored layered material. The lead tin disulfide crystallizes in orthorhombic structure (*Pnma* space group) that is presented in Fig. 1a. The S atoms are bonded to Pb or Sn atoms and together are forming puckered bilayers, approximately 0.6 nm thick.[10] Each bilayer is separated from another by approximately 0.28 nm.[10]

The first report about lead tin disulfide comes from 1904[11] where the study of teallite (naturally occurring lead tin disulfide) including the general crystallographic character and basic physical properties, like hardness and ability to cleavage, were shown. Other reports bring information about the PbS-SnS mixed crystals,[12] in which due to their high miscibility are two binary compounds of which $PbSnS_2$ is composed. Interestingly, this material could be used for promising potential application. Firstly, due to its 1.4 eV band gap, it was recognized as a potential candidate as a material for thin film solar cells.[12,13] Lately, it was demonstrated that $PbSnS_2$ can be utilized as a part of thermoelectric composite material, collectively with PbTe.[14] Incorporation of $PbSnS_2$ into PbTe structure results in decreasing of the lattice thermal conductivity down to 0.4 $Wm^{-1}K^{-1}$,[10] in which low value is crucial for thermoelectric devices.

However, up to date, there are few information about various properties of this material, especially about their phonon properties.

The phonon properties can be studied by using Raman spectroscopy, which is an excellent nondestructive tool for characterization of structural,[15] thermal,[16,17] optical[18] and electronic[19,20] properties of layered materials. The temperature-dependent Raman measurements can be used as a tool to investigate vibration, transport, phonon–phonon properties or electron–phonon interactions,[21] and angle-dependent Raman spectra can be used for assignment of Raman modes or crystal orientation.[22]

Here in this work, we report, for the first time, Raman measurements of $PbSnS_2$ thin films obtained by mechanical exfoliation from single crystal. We compare lead tin disulfide Raman spectra for different incident excitation wavelengths and different polarization configurations. Further, we present temperature-dependent (80–400 K) Raman spectra measurements. From polarization-dependent measurements, we show that this material has anisotropic optical properties. The temperature-dependent studies revealed nonlinear dependence of phonon behaviour (both modes' position and widths) that stems from optical phonon decay into two or three acoustic phonons. We also found that extracted first-order temperature coefficients are among the largest for layered materials. Our studies can be further used for investigation of other

* *Correspondence to: Mariusz Zdrojek, Faculty of Physics, Warsaw University of Technology, Koszykowa 75, 00-662 Warsaw, Poland. E-mail: zdrojek@if.pw.edu.pl*

† *These authors contributed equally to this work.*

a *Faculty of Physics, Warsaw University of Technology, Koszykowa 75, 00-662, Warsaw, Poland*

b *Faculty of Chemistry, Warsaw University of Technology, Noakowskiego 3, 00-664, Warsaw, Poland*

c *Institute of Electron Technology, Warsaw, Poland and with Institute of Microelectronics and Optoelectronics, Warsaw University of Technology, Warsaw, Poland*

Copyright © 2016 John Wiley & Sons, Ltd.

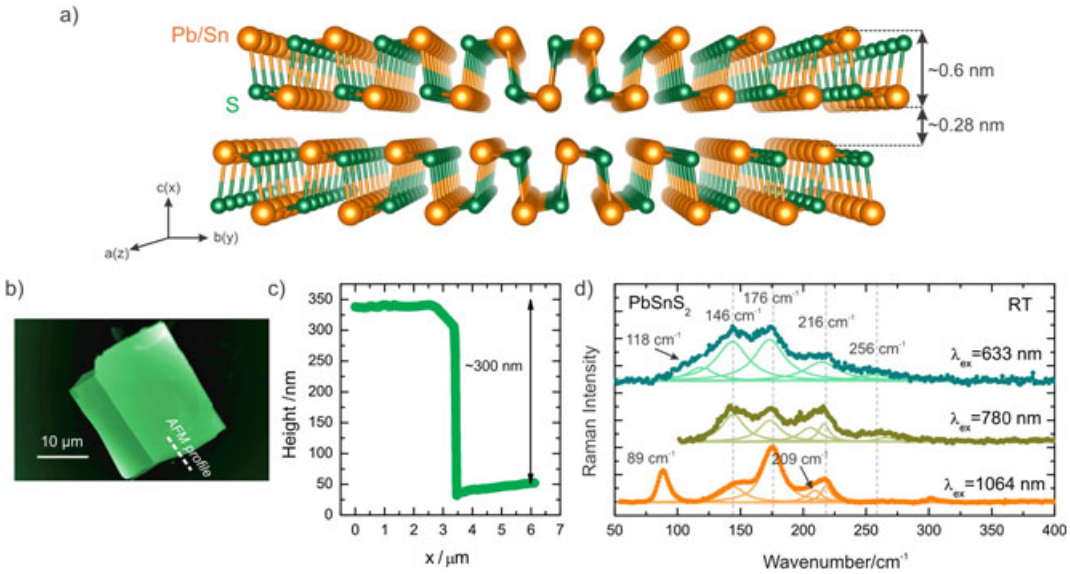

Figure 1. (a) Crystal structure of $PbSnS_2$, (b) atomic force microscope image and (c) height profile of $PbSnS_2$ flake with thickness ~300 nm. (d) Raman spectra of $PbSnS_2$ obtained with $\lambda_{ex} = 633$, 780 and 1064 nm under circular polarization. [Colour figure can be viewed at wileyonlinelibrary.com]

properties of $PbSnS_2$ and may be useful for application of this material in thermoelectric, electrical or optical devices.

Experimental methods

$PbSnS_2$ thin flakes were fabricated by conventional mechanical exfoliation technique[1] from commercially available (2D semiconductors) single crystals and transferred into thermally oxidized Si substrates covered with 285-nm-thick SiO_2 layer. Prior to Raman measurements, the fabricated flakes were characterized by atomic force microscopy (AFM). The example image of fabricated film and height profile is shown in Fig. 1b, c. The thickness of fabricated flakes was typically about 200–300 nm. Room temperature Raman spectra were recorded by using three different excitation lines λ_{ex}: 633 nm (1.96 eV) He–Ne laser line, 1064 nm (1.16 eV) neodymium-doped yttrium aluminium garnet laser line by Renishaw inVia Raman microscope and 780 nm (1.59 eV) diode laser by Thermo Nicolet Almega XR Raman spectrometer. Temperature-dependent and polarized Raman measurements were taken by using 1064 nm (1.16 eV) neodymium-doped yttrium aluminium garnet excitation wavelength. The signal was collected by using 50× (numerical aperture 0.5) and 100× objectives (numerical aperture 0.85) giving the laser spot size much smaller than film size. The laser power, calibrated on the sample, was kept low (<0.2 mW) in order to avoid unintentional additional heating of the sample. The temperature-dependent Raman measurements were performed in optical cryostat (Oxford Instrument) in 80–400 K range with 20 K step (stability ~0.1 K). The polarized measurements were performed as a function of the angle between polarization vectors of incident and scattered light (from 0° to 180° with 5° step) in backscattering geometry and in VV (the scattered and the incident light are parallel to each other) and VH (the scattered and the incident light are perpendicular to each other) polarization configurations. The measurements for each temperature were performed several times and in different places on the flake to minimize any statistical variation. All recorded Raman spectra were fitted by using Levenberg–Marquardt algorithm with Lorentzian shape function. The temperature-dependent and the angle-dependent measurements presented in this work were performed on the same flake. The same measurements were performed on different flakes with similar thickness, and we did not observe any significant differences.

Results and discussion

Room temperature multiwavelength Raman spectra of $PbSnS_2$

The room temperature (circular polarized) Raman spectra obtained with different excitation wavelengths of 633, 780 and 1064 nm are shown in Fig. 1d. We have identified five Raman bands in spectrum for $\lambda_{ex} = 633$ nm with maxima located at 118, 146, 176, 216 and 256 cm^{-1}. In the spectrum for $\lambda_{ex} = 780$ nm, we have observed four bands: 149, 178, 216 and 256 cm^{-1}. For $\lambda_{ex} = 1064$ nm, we observed five bands at 89, 146, 176 and 216 cm^{-1}. We note that spectra taken with $\lambda_{ex} = 1064$ nm are much sharper and with highest signal-to-noise ratio as compared with other used excitation wavelengths, probably due to resonance between phonon energy (1.165 eV) and energy to an electronic transition.[23] However, more detailed studies[24] need to be taken in order to study the resonance effect in $PbSnS_2$. The Raman bands located at 146, 176 and 216 cm^{-1} are present in spectra taken for all used λ_{ex}. The mode at 256 cm^{-1} band is present only in spectra obtained for $\lambda_{ex} = 633$ and 780 nm. Whereas, the mode located at 89 cm^{-1} seen in 1064 nm spectrum is not visible in spectra for other excitation wavelengths (partially due to limitation of experimental set-up). The Raman bands that appeared in at least two of the measured spectra are not dispersive (see dashed red horizontal lines in Fig. 1). For convenience, in this work, the observed Raman bands are named after their position at room temperature.

Up to date, there is no report in the literature devoting to $PbSnS_2$ Raman spectra; thus, obtained results were compared with the spectra of the two compounds from which teallite is formed – SnS and PbS. PbS crystallizes in cubic structure (galena) at ambient pressure and undergoes phase transition to the orthorhombic structure at high pressures. However, the space group (*Cmca* or *Pnma*) of orthorhombic structure of PbS is under debate.[25] Up to

Copyright © 2016 John Wiley & Sons, Ltd.

date, only one pressure-dependent Raman study of PbS was reported; however, obtained Raman spectra were not conclusive about structure type.[26]

Taking this into consideration, the Raman spectra of PbS and $PbSnS_2$ cannot be directly compared at this stage. Raman study of SnS shows[27,28] four bands in the spectrum ~94, ~189 and 218 cm^{-1} of A_g[29] symmetry and ~157 cm^{-1} of B_{3g}[29] symmetry (for $\lambda_{ex}=633$ nm). For longer radiation wavelength $\lambda_{ex}=780$ nm), Raman spectrum of SnS exhibits two bands: 194 and 218 cm^{-1}.[30] The bands ~94, ~157, ~185 and 218 cm^{-1} may correspond to 89, 146, 176 and 216 cm^{-1} bands from our spectra, respectively. No Raman measurements for $\lambda_{ex}=1064$ nm for SnS were found in the literature; however, the shape of Raman spectra was similar to the spectra of SnSe taken with $\lambda_{ex}=633$ nm.[27] The ~118, ~209 and ~256 cm^{-1} bands may be related to PbS-like modes in $PbSnS_2$. The comparison of our data with the literature concerning discussed compounds is given in Table 1. We can carefully conclude that there are some similarities between SnS and $PbSnS_2$ Raman bands' position, which has the same crystal structure but bearing in mind that atomic distances in this materials may be slightly different resulting in a change in the photon energy.

Angle-dependent Raman spectra of $PbSnS_2$

In order to fully determine the symmetry of observed Raman modes, we have performed full polarization measurements for $\lambda_{ex}=1064$. The measurements were performed with two polarization configuration: VV ($\mathbf{e_i} \parallel \mathbf{e_s}$) and VH ($\mathbf{e_i} \perp \mathbf{e_s}$), where $\mathbf{e_i}$ and $\mathbf{e_s}$ are unitary vectors of incident and scattered light polarizations. The obtained polarization-dependent relation between measured band intensities and polarization angle of incident and scattered light was analysed by using Raman tensor of Raman modes of $PbSnS_2$ orthorhombic phase (D_{2h} space group)[31]:

$$R(A_g)=\begin{pmatrix} A & 0 & 0 \\ 0 & B & 0 \\ 0 & 0 & C \end{pmatrix}, R(B_{1g})=\begin{pmatrix} 0 & D & 0 \\ D & 0 & 0 \\ 0 & 0 & 0 \end{pmatrix}$$
$$R(B_{2g})=\begin{pmatrix} 0 & 0 & E \\ 0 & 0 & 0 \\ E & 0 & 0 \end{pmatrix}, R(B_{3g})=\begin{pmatrix} 0 & 0 & 0 \\ 0 & 0 & F \\ 0 & F & 0 \end{pmatrix} \quad (1)$$

The intensities of Raman modes are proportional to $|\mathbf{e_i} R \mathbf{e_s}|^2$, where R is the Raman tensor of given mode. We used notation after Chandrasekhar et al.,[29] i.e. direction of incident and scattered light is along c-axis (x-axis in our experimental set-up) of the crystal (Fig. 1a). The unitary vectors may be expressed as $\mathbf{e_i}=(0, \cos\theta, \sin\theta)$, whereas $\mathbf{e_s}=(0, \cos\theta, \sin\theta)$ and $(0, -\sin\theta, \cos\theta)$ for VV and VH polarization, respectively. Considering the form of these vectors for VV and VH polarization, the theoretical relation of Raman mode intensity *versus* polarization angle for A_g and B_{3g} modes, which are allowed in used geometry, takes the form[31]

$$\begin{aligned} I(A_g, VV) &= \left(B\cos^2\theta + C\sin^2\theta\right)^2 \\ I(B_{3g}, VV) &= F^2\sin^2 2\theta \\ I(A_g, VH) &= \frac{(C-B)^2}{4}\sin^2 2\theta \\ I(B_{3g}, VH) &= F^2\cos^2 2\theta \end{aligned} \quad (2)$$

Figure 2 shows polarization-dependent relation between measured normalized band intensities and polarization angle of incident and scattered light along with fit of Eqn (2) to experimental data.

It should be noted that observed Raman modes show strong angular dependence of their intensities. The measured data fit quite well to the theoretical dependence (Eqn (2)). Some discrepancies at 90° (intensity not going to 0) for VH polarization for 89, 176 and 216 cm^{-1} modes can stem from polarization misalignment in our set-up. Nevertheless, we can conclude that observed Raman modes at 89, 176 and 216 cm^{-1} belong to A_g symmetry, and mode observed at 146 cm^{-1} belongs to B_{3g} symmetry. It should be noted that theoretical and experimental curves for Ag modes are shifted of some angle that may result from misalignment between incident light and armchair direction (along b-axis) of the crystal.[31]

Table 1. Summary of obtained band positions in Raman spectra for radiation wavelength of 633, 780 and 1064 nm and comparison to bands occurring in SnS spectra for the same wavelength radiation

Material	$\lambda_{ex}=633$ nm	$\lambda_{ex}=780$ nm	$\lambda_{ex}=1064$ nm
$PbSnS_2$, this work	—	—	89 cm^{-1}
	118 cm^{-1}	—	—
	146 cm^{-1}	146 cm^{-1}	146 cm^{-1}
	176 cm^{-1}	176 cm^{-1}	176 cm^{-1}
	—	209 cm^{-1}	209 cm^{-1}
	216 cm^{-1}	216 cm^{-1}	216 cm^{-1}
	256 cm^{-1}	256 cm^{-1}	—
SnS	A_g, ~94 cm^{-1}	—	—
	B_{3g}, ~157 cm^{-1}	—	—
	B_{3g}, ~185 cm^{-1}	~194 cm^{-1}	—
	B_{3g}, ~218 cm^{-1}	~218 cm^{-1}	—

Temperature-dependent Raman spectra of $PbSnS_2$

To study temperature phonon behaviour, temperature-dependent Raman measurements were conducted. Figure 3a shows the temperature evolution of the $PbSnS_2$ Raman spectra taken with $\lambda_{ex}=1064$ nm. The Raman modes tend to strong broadening and softening with the increasing temperature (see vertical line for eye guidance). The detailed temperature evolution of Raman positions and full width at half maximum (FWHM) is depicted in the Fig. 3b–h, where the strong shift of the Raman modes and strong nonlinearity of Raman modes' positions and widths are observed. The total modes' position shifts from T = 80 to 400 K are for 146 cm^{-1} mode – 6 cm^{-1}, for 176 cm^{-1} mode – 13 cm^{-1} and for the 216 cm^{-1} mode – 14 cm^{-1}. The temperature dependence of the position of 89 cm^{-1} Raman mode is relatively weak in comparison with other modes, and nonlinearity is not observed (Fig. 3b). The error bars were calculated as expanded uncertainty at the 95% level of confidence and include finite spectral resolution and the average uncertainty of determination of peak position (~0.1 cm^{-1}) or FWHM (~0.2 cm^{-1}).

To describe temperature dependence of positions and widths of 146, 176 and 216 cm^{-1} Raman modes, we first used approach proposed by Balkanski et al.[32] that is based on the phenomenon of optical phonon decay into two or three acoustic phonons with equal energies due to cubic and quartic anharmonicity of lattice potential. This approach has been successfully used to describe temperature dependence of other layered materials, like WTe_2,[33] monolayer MoS_2,[34] $ReSe_2$ and $SnSe_2$ thin flakes[35] as well as to

Copyright © 2016 John Wiley & Sons, Ltd.

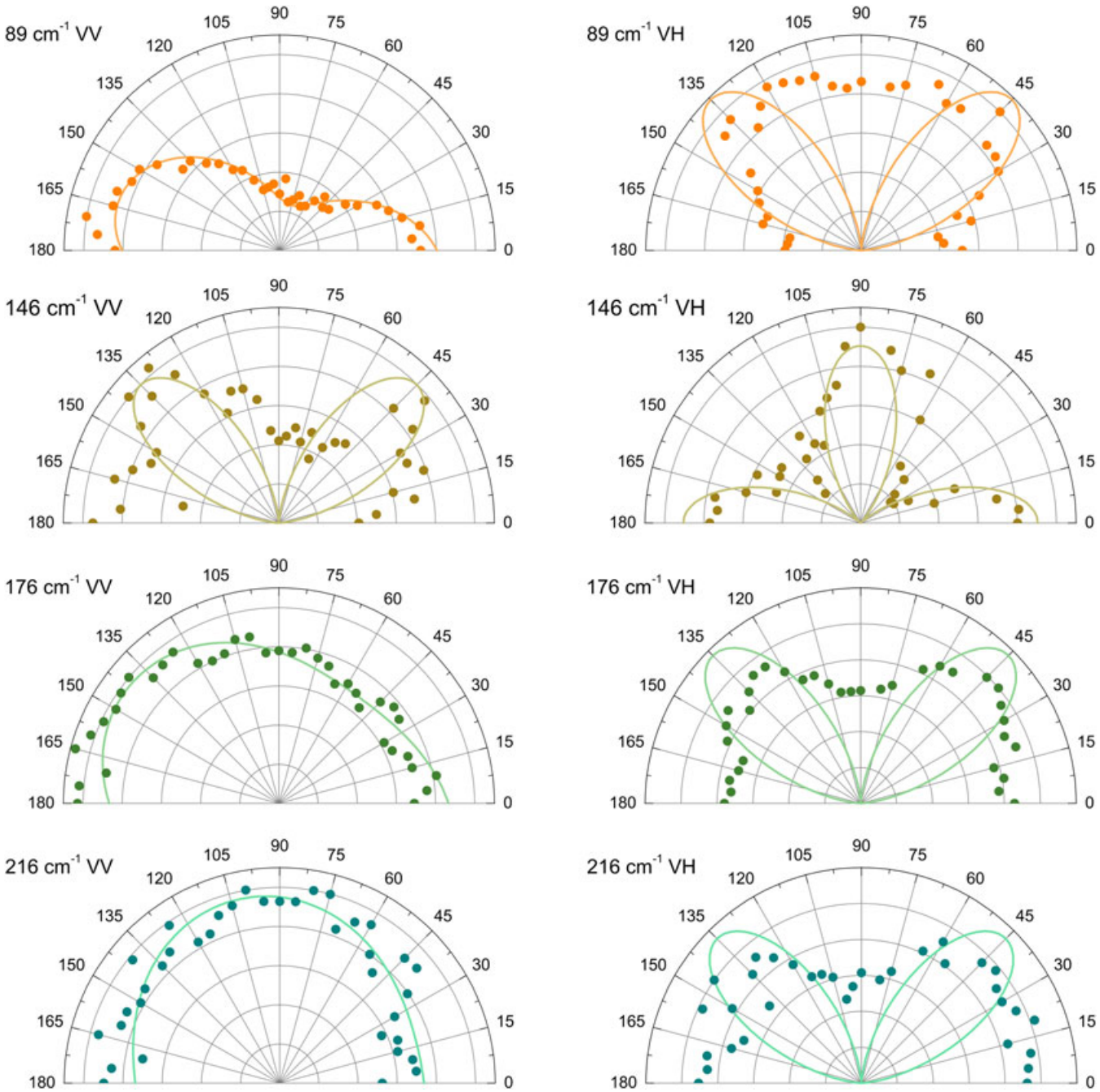

Figure 2. Normalized integrated intensities of $PbSnS_2$ Raman modes for different polarization angle measured with $\lambda_{ex} = 1064$ nm in VV and VH configuration. [Colour figure can be viewed at wileyonlinelibrary.com]

carbon nanotube thin films.[36] To fit experimental data for phonon shifts and FWHMs, we use expressions[32]

$$\omega(T) = \omega_0 + A\left(1 + \frac{2}{e^x - 1}\right) + B\left(1 + \frac{3}{e^y - 1} + \frac{3}{(e^y - 1)^2}\right) \quad (3)$$

$$\Gamma(T) = \Gamma_0 + C\left(1 + \frac{2}{e^x - 1}\right) + D\left(1 + \frac{3}{e^y - 1} + \frac{3}{(e^y - 1)^2}\right) \quad (4)$$

where $x = \omega_0/2k_bT$, $y = \omega_0/3k_bT$, ω_0 is the peak position at temperature extrapolated to 0 K and is Planck constant divided by 2π, k_b is Boltzmann constant, A, B, C and D are anharmonic constants and Γ_0 is the temperature-independent broadening due to disorder of crystal or strain.[37] In Eqns (3) and (4), second terms correspond to three and third terms to four-phonon processes. The values of obtained anharmonic constants are presented in Table 2. Moreover, also the FWHMs tend to nonlinear behaviour with increasing temperature, and the four-phonon process model is easily fitted to the obtained data. As it is shown in Fig. 3c–e, strongly nonlinear behaviour of peak position stems from mentioned phonon decay. The ratios of anharmonic constants B/A and D/C are relatively small and have the values 0.35, 0.18 and 0.3 (B/A) and 0.17, 0.26 and 0.031 (D/C) for 146, 176 and 216 cm^{-1} modes, respectively, as the probability of three-phonon process is larger than four-phonon process. We note that apart from anharmonicity, the volume thermal expansion of the lattice could also contribute to the increase of mode

Copyright © 2016 John Wiley & Sons, Ltd.

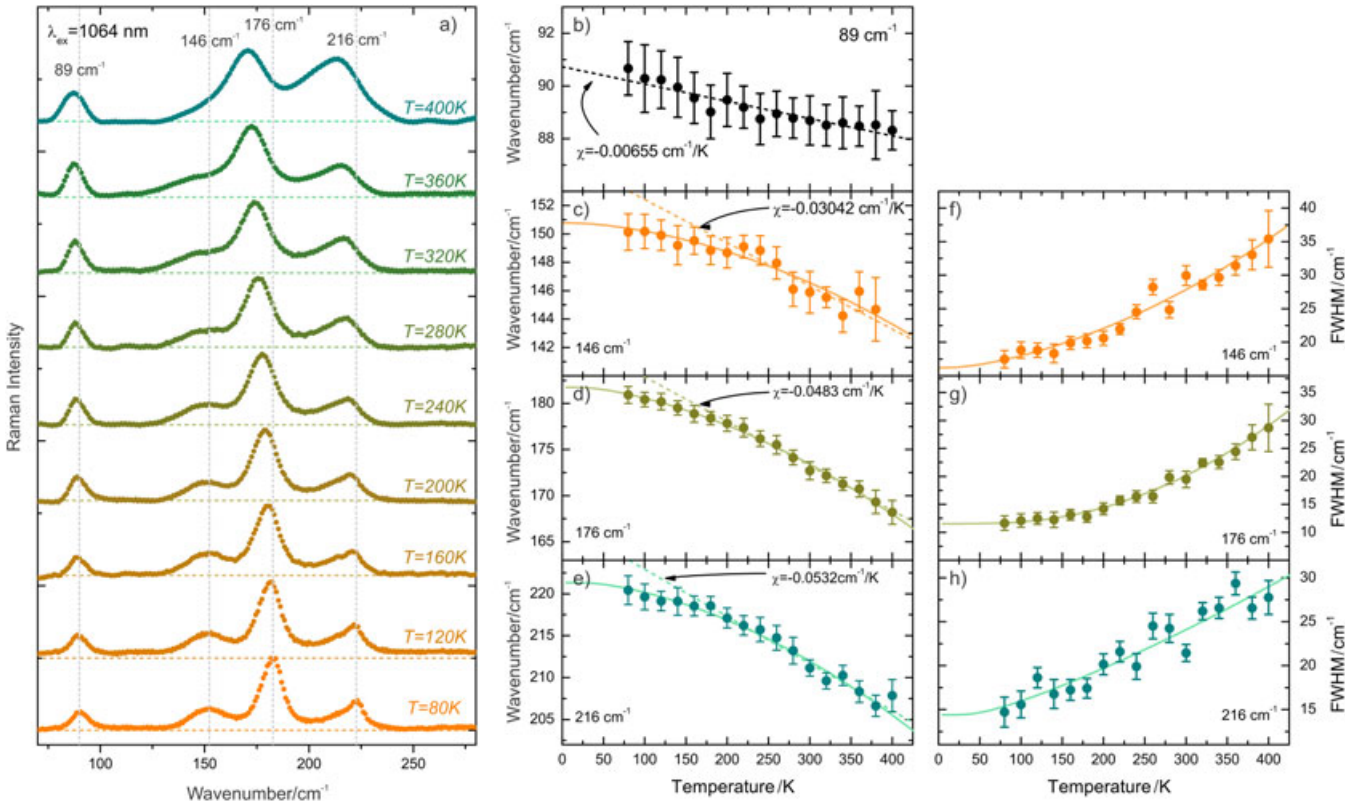

Figure 3. (a) Selected Raman spectra (λ_{ex} = 1064 nm) of $PbSnS_2$ measured in 80−400 K temperature range. (b) Temperature dependence of 89 cm cm^{-1} $PbSnS_2$ Raman mode. Temperature dependence of 146, 176 and 216 cm^{-1} $PbSnS_2$ Raman modes. (c–e) Positions and (f–h) FWHMs. [Colour figure can be viewed at wileyonlinelibrary.com]

Table 2. The values of anharmonic constants obtained from the analysis of temperature dependence of Raman mode positions and widths

Mode	ω_0 (cm^{-1})	A (cm^{-1})	B (cm^{-1})	Γ_0 (cm^{-1})	C (cm^{-1})	D (cm^{-1})
146 cm^{-1}	150.885	−0.1824	−0.064	15.24	0.833	0.148
176 cm^{-1}	182.71	−0.82	−0.15	12.68	−1.59	0.415
216 cm^{-1}	222.54	−0.935	−0.286	11.58	2.724	0.0841

widths and to the decrease of mode positions with increasing temperature.[38] Up to know, there is no information about theoretical or experimental values of coefficient of linear thermal expansion and Grüneisen parameter of $PbSnS_2$ from which thermal expansion contribution can be calculated; however, this for many layered material can be neglected.[33,34,39]

For the temperatures above approx. 220 K, the temperature dependence of mode position tends to linear dependence, and first-order temperature coefficient was calculated, corresponding to the Eqn (5):

$$\omega(T) = \omega_0 + \chi T \quad (5)$$

where ω_0 is the phonon wavenumber at temperature interpolated to 0 K and χ is the first-order temperature coefficient. The obtained values are summarized in Table S1 (Supporting Information). The first-order temperature coefficient can be used in the optothermal method for the determination of the thermal conductivity[40] or for the in-operando measurements of the temperature rise in electronic devices.[41] As shown in Fig. 3b, the 89 cm^{-1} mode shows rather weak temperature dependence, the phonon wavenumber changes of about, and extracted χ value was about −0.00655 cm^{-1} K^{-1}. Obtained values of first-order temperature coefficients for 146, 176 and 216 cm^{-1} modes are −0.0304, −0.0483 and −0.0563 cm^{-1} K^{-1}, which are much higher than the values for other layered materials. The reported χ values for other layered materials are summarized in Table S1. The χ value for the supported monolayer MoS_2 was reported to be 0.0178 cm^{-1} K^{-1} for A_{1g} mode[34] and −0.013 cm^{-1} K^{-1} for multilayer film. For few layer black phosphorus where relatively strong temperature dependence of Raman spectra was reported,[42,43] χ values are −0.01642, −0.02707 and −0.02833 cm^{-1} K^{-1} for A_{1g}, B_{2g} and A_{2g} modes, respectively.[43] It is noteworthy that layered materials that crystallize in orthorhombic structure, i.e. SnSe, BP, GeSe or $PbSnS_2$, possess noticeably higher first-order temperature coefficients of Raman modes than other layered materials with hexagonal (MoS_2, WS_2, $SnSe_2$) or triclinic structure ($ReSe_2$).[31,33–35,39,42–46]

Conclusions

We have performed the Raman spectroscopy studies of the teallite – $PbSnS_2$ thin films. The full polarization measurement performed in the VV and VH configuration showed strong angular dependency of Raman mode intensities and allowed to determine mode symmetries. The observed Raman modes at 89, 176, and 216 cm^{-1} belong to A_g symmetry, and 146 cm^{-1} mode belongs to B_{3g} symmetry. The strong nonlinear dependence of 146, 176 and 216 cm^{-1} modes observed in the temperature dependency of the Raman spectra was attributed to the optical phonon decay

Copyright © 2016 John Wiley & Sons, Ltd.

onto two or three acoustic phonons. Extracted first-order temperature coefficients for 146, 176 and 216 cm^{-1} modes were −0.0304, −0.0483 and −0.0563 $cm^{-1} K^{-1}$, respectively, which are among the largest reported for layered materials. Our studies may be useful for further characterization properties of $PbSnS_2$, especially thermal conductivity or interfacial thermal conductance,[17,47,48] and suggest that $PbSnS_2$ possess anisotropic character of optical, thermal and electrical properties as similar to other orthorhombic layered materials.[22,31,49]

Acknowledgements

The work was supported by the Polish Ministry of Science and Higher Education within the Diamond Grant programme (0025/DIA/2013/42) and by Faculty of Physics WUT statutory work. A.Ł., M.W. and J.J. thank the Polish National Science Centre for support within project 2014/15/D/ST5/03944. A.Ł. thanks the National Centre of Science for the support within project 2015/19/N/ST5/02312.

References

[1] D. J. Late, *Adv. Device Mater.* **2015**, *1*, 52.
[2] K. S. Novoselov, A. K. Geim, S. V. Morozov, D. Jiang, Y. Zhang, S. V. Dubonos, I. V. Grigorieva, A. A. Frisov, *Science* **2004**, *306*, 666.
[3] Q. H. Wang, K. Kalantar-Zadeh, A. Kis, J. N. Coleman, M. S. Strano, *Nat. Nanotechnol.* **2012**, *7*, 699.
[4] A. S. Pawbake, M. S. Pawar, S. R. Jadkar, D. J. Late, *Nanoscale* **2016**. DOI:10.1039/C5NR07401K.
[5] D. J. Late, P. A. Shaikh, R. Khare, R. V. Kashid, M. Chaudhary, M. A. More, S. B. Ogale, *ACS Appl. Mater. Interfaces* **2014**, *6*, 15881.
[6] M. B. Erande, M. S. Pawar, D. J. Late, *ACS Appl. Mater. Interfaces* **2016**, *8*, 11548.
[7] X. Ling, H. Wang, S. Huang, F. Xia, M. S. Dresselhaus, *Proc. Natl. Acad. Sci.* **2015**201416581.
[8] A. S. Pawbake, J. O. Island, E. Flores, J. R. Ares, C. Sanchez, I. J. Ferrer, S. R. Jadkar, H. S. J. van der Zant, A. Castellanos-Gomez, D. J. Late, *ACS Appl. Mater. Interfaces* **2015**, *7*, 24185.
[9] U. S. Shenoy, U. Gupta, D. S. Narang, D. J. Late, U. V. Waghmare, C. N. R. Rao, *Chem. Phys. Lett.* **2016**, *651*, 148.
[10] S. N. Girard, T. C. Chasapis, J. He, X. Zhou, E. Hatzikraniotis, C. Uher, K. M. Paraskevopoulos, V. P. Dravid, M. G. Kanatzidis, *Energy Environ. Sci.* **2012**, *5*, 8716.
[11] G. T. Prior, *Z Krist. Miner.* **1904**, *14*, 21.
[12] D. M. Unuchak, K. Bente, G. Kloess, W. Schmitz, V. F. Gremenok, V. A. Ivanov, V. Ukhov, *Phys. Status Solidi C* **2009**, *6*, 1191.
[13] B. Thangaraju, P. Kaliannan, *Cryst Res Technol* **2000**, *35*, 71.
[14] J. He, S. N. Girard, J.-C. Zheng, L. Zhao, M. G. Kanatzidis, V. P. Dravid, *Adv. Mater.* **2012**, *24*, 4440.
[15] D. J. Late, B. Liu, H. S. S. R. Matte, C. N. R. Rao, V. P. Dravid, *Adv. Funct. Mater.* **2012**, *22*, 1894.
[16] J. Judek, A. P. Gertych, M. Świniarski, A. Łapińska, A. Dużyńska, M. Zdrojek, *Sci. Rep.* **2015**, *5*, 12422.
[17] A. Taube, J. Judek, A. Łapińska, M. Zdrojek, *ACS Appl. Mater. Interfaces* **2015**, *7*, 5061.
[18] H. B. Ribeiro, M. A. Pimenta, C. J. S. de Matos, R. L. Moreira, A. S. Rodin, J. D. Zapata, E. A. T. de Souza, A. H. Castro Neto, *ACS Nano* **2015**, *9*, 4270.
[19] B. Chakraborty, A. Bera, D. V. S. Muthu, S. Bhowmick, U. V. Waghmare, A. K. Sood, *Phys. Rev. B* **2012**, 85. DOI:10.1103/PhysRevB.85.161403.
[20] L. Sun, J. Yan, D. Zhan, L. Liu, H. Hu, H. Li, B. K. Tay, J.-L. Kuo, C.-C. Huang, D. W. Hewak, P. S. Lee, Z. X. Shen, *Phys. Rev. Lett.* **2013**, 111. DOI:10.1103/PhysRevLett.111.126801.
[21] D. J. Late, U. Maitra, L. S. Panchakarla, U. V. Waghmare, C. N. R. Rao, *J. Phys. Condens. Matter* **2011**, *23*, 055303.
[22] J. Wu, N. Mao, L. Xie, H. Xu, J. Zhang, *Angew. Chem. Int. Ed.* **2015**, *54*, 2366.
[23] F.-Y. Ran, Z. Xiao, Y. Toda, H. Hiramatsu, H. Hosono, T. Kamiya, *Sci. Rep.* **2015**, *5*, 10428.
[24] T. T. K. Chi, G. Gouadec, P. Colomban, G. Wang, L. Mazerolles, N. Q. Liem, J. Raman, *Spectrosc.* **2011**, *42*, 1007.
[25] Y. Li, C. Lin, J. Xu, G. Li, X. Li, J. Liu, *AIP Adv.* **2014**, *4*, 127112.
[26] Y. S. Ponosov, S. V. Ovsyannikov, S. V. Streltsov, V. V. Shchennikov, K. Syassen, *High Press. Res.* **2009**, *29*, 224.
[27] M. Devika, N. Koteeswara Reddy, M. Prashantha, K. Ramesh, S. Venkatramana Reddy, Y. B. Hahn, K. R. Gunasekhar, *Phys. Status Solidi A* **2010**, *207*, 1864.
[28] G. Barone, T. G. Hibbert, M. F. Mahon, K. C. Molloy, L. S. Price, I. P. Parkin, A. M. E. Hardy, M. N. Field, *J. Mater. Chem.* **2001**, *11*, 464.
[29] H. R. Chandrasekhar, R. G. Humphreys, U. Zwick, M. Cardona, *Phys. Rev. B.* **1977**, *15*, 2177.
[30] S. Cheng, C. Huang, G. Chen, G. J. Conibeer, in *Proc SPIE* (Eds: J.-C. Chiao, A. S. Dzurak, C. Jagadish, D. V. Thiel), **2006** 641512–641512–8.
[31] J. Xia, X.-Z. Li, X. Huang, N. Mao, D.-D. Zhu, L. Wang, H. Xu, X.-M. Meng, *Nanoscale* **2016**, *8*, 2063.
[32] M. Balkanski, R. F. Wallis, E. Haro, *Phys. Rev. B.* **1983**, *28*, 1928.
[33] W.-D. Kong, S.-F. Wu, P. Richard, C.-S. Lian, J.-T. Wang, C.-L. Yang, Y.-G. Shi, H. Ding, *Appl. Phys. Lett.* **2015**, *106*, 081906.
[34] A. Taube, J. Judek, C. Jastrzębski, A. Duzynska, K. Świtkowski, M. Zdrojek, *ACS Appl. Mater. Interfaces* **2014**, *6*, 8959.
[35] A. Taube, A. Łapińska, J. Judek, M. Zdrojek, *Appl. Phys. Lett.* **2015**, *107*, 013105.
[36] A. Duzynska, J. Judek, M. Zdrojek, *Appl. Phys. Lett.* **2014**, *105*, 213105.
[37] Z. D. Dohčević-Mitrović, M. Radović, M. Šćepanović, M. Grujić-Brojčin, Z. V. Popović, B. Matović, S. Bošković, *Appl. Phys. Lett.* **2007**, *91*, 203118.
[38] M. Thripuranthaka, R. V. Kashid, C. Sekhar Rout, D. J. Late, *Appl. Phys. Lett.* **2014**, *104*, 081911.
[39] A. Taube, A. Łapińska, J. Judek, N. Wochtman, M. Zdrojek, *J. Phys. Appl. Phys.* **2016**, *49*, 315301.
[40] A. A. Balandin, S. Ghosh, W. Bao, I. Calizo, D. Teweldebrhan, F. Miao, C. N. Lau, *Nano Lett.* **2008**, *8*, 902.
[41] Z. Yan, G. Liu, J. M. Khan, A. A. Balandin, *Nat. Commun.* **2012**, *3*, 827.
[42] S. Zhang, J. Yang, R. Xu, F. Wang, W. Li, M. Ghufran, Y.-W. Zhang, Z. Yu, G. Zhang, Q. Qinothers, *ACS Nano* **2014**, *8*, 9590.
[43] A. Łapińska, A. Taube, J. Judek, M. Zdrojek, *J. Phys. Chem. C* **2016**, *120*, 5265.
[44] N. A. Lanzillo, A. G. Birdwell, M. Amani, F. J. Crowne, P. B. Shah, S. Najmaei, Z. Liu, P. M. Ajayan, J. Lou, M. Dubey, S. K. Nayak, T. P. O'Regan, *Appl. Phys. Lett.* **2013**, *103*, 093102.
[45] M. Thripuranthaka, D. J. Late, *ACS Appl. Mater. Interfaces* **2014**, *6*, 1158.
[46] D. J. Late, S. N. Shirodkar, U. V. Waghmare, V. P. Dravid, C. N. R. Rao, *ChemPhysChem* **2014**, *15*, 1592.
[47] A. A. Balandin, *Nat. Mater.* **2011**, *10*, 569.
[48] I. Calizo, S. Ghosh, W. Bao, F. Miao, C. Ning Lau, A. A. Balandin, *Solid State Commun.* **2009**, *149*, 1132.
[49] Z. Luo, J. Maassen, Y. Deng, Y. Du, R. P. Garrelts, M. S. Lundstrom, P. D. Ye, X. Xu, *Nat. Commun.* **2015**, *6*, 8572.

Supporting information

Additional supporting information may be found in the online version of this article at the publisher's web site.

Copyright © 2016 John Wiley & Sons, Ltd.